Water Science & Technology

Water Science & Technology Vol 89 No 2, 225 doi: 10.2166/wst.2024.007

Fluoranthene degradation in a persulfate system activated by sulfidated nano zero-valent iron (S-nZVI): performance and mechanisms

Ruzhuang Zhang[a], Yi Zhu[a], Jiaqi Dong[b], Zhennan Yao[a], Guilu Zeng[b], Xianxian Sheng[b], Ziqian Xu[a] and Shuguang Lyu[b,*]

[a] Shanghai Chengtou Environmental Ecological Remediation Technology Co., LTD, Shanghai 200331, China
[b] State Environmental Protection Key Laboratory of Environmental Risk Assessment and Control on Chemical Process, East China University of Science and Technology, Shanghai 200237, China
*Corresponding author. E-mail: lvshuguang@ecust.edu.cn

ABSTRACT

Fluoranthene (FLT) has received mounting focus due to its hazardous properties and frequent occurrence in groundwater. In this study, sulfidated nano zero-valent iron (S-nZVI) was selected as an efficient catalyst for activating persulfate (PS) to degrade FLT. The effects of reagent doses, various water conditions (pH, anions, and humic acid), and the presence of surfactants on FLT degradation were investigated. Radical probe experiments, electron paramagnetic resonance (EPR) spectrum detection, and scavenging tests were performed to identify the major reactive oxygen species (ROS) in the system. The results showed that in the PS/S-nZVI system, 96.2% of FLT was removed within 120 min at the optimal dose of PS = 0.07 mM and S-nZVI = 0.0072 g L^{-1}. S(-II) in the S-nZVI surface layer promoted Fe(II) regeneration. Furthermore, HO• and $SO_4^{-\bullet}$ were identified as the main contributors to FLT degradation. The intermediates of FLT degradation were detected by gas chromatograph-mass spectrometry (GC-MS) and a possible FLT degradation pathway was proposed. Finally, the effective degradation of two other common polycyclic aromatic hydrocarbons (PAHs) (naphthalene and phenanthrene) demonstrated the broad-spectrum reactivity of the PS/S-nZVI process. In conclusion, these findings strongly demonstrate that the PS/S-nZVI process is a promising alternative for the remediation of PAH-contaminated groundwater.

Key words: fluoranthene, groundwater remediation, persulfate, polycyclic aromatic hydrocarbons, sulfidated nano zero-valent iron

HIGHLIGHTS

- HO• and $SO_4^{-\bullet}$ were the primary ROS in the PS/S-nZVI system for FLT degradation.
- The possible degradation pathway of FLT was proposed.
- The S(-II) enhancement mechanism was fully described.
- Efficient FLT degradation in actual groundwater was achieved.
- The broad-spectrum reactivity of the PS/S-nZVI system was investigated for other PAHs removal.

GRAPHICAL ABSTRACT

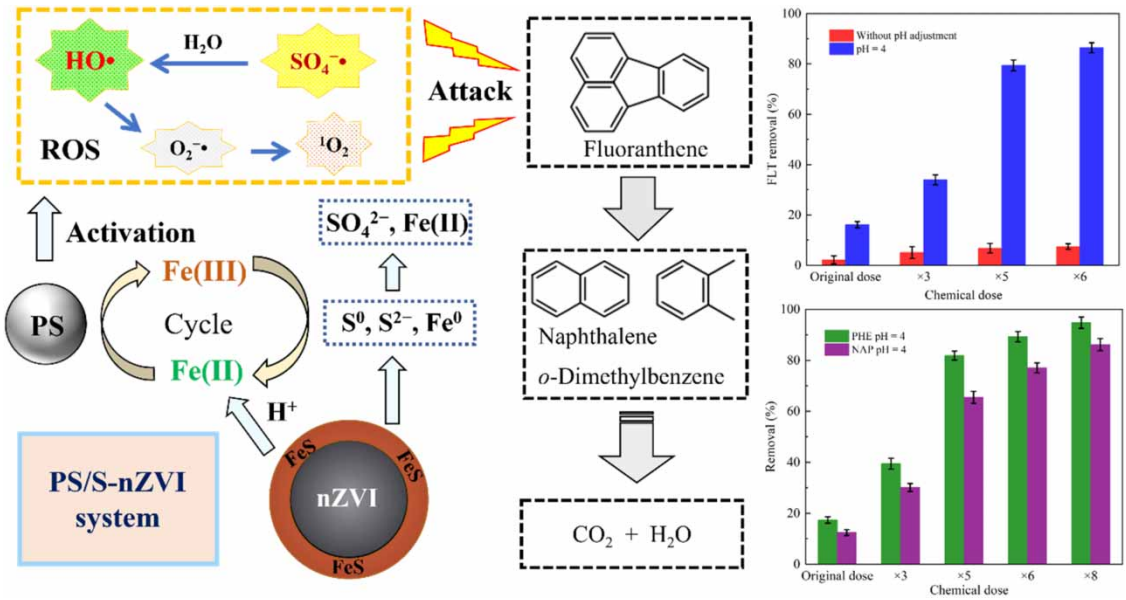

1. INTRODUCTION

Polycyclic aromatic hydrocarbons (PAHs) are a type of persistent organic pollutants that have caused widespread harm due to their toxicity and difficulty in natural degradation (Liu *et al.* 2021; Samrendra *et al.* 2023). The poor degradability of PAHs originating from inadequate combustion of fossil fuels and biomass is mainly attributed to their composition of at least two linear or aggregated fused aromatic rings (Mojiri *et al.* 2019). Fluoranthene (FLT), as a representative pollutant of PAHs with three benzene rings and a central five-membered ring, is detected frequently in contaminated groundwater. FLT is one of the 16 PAHs that is listed as priority pollutants by the United States Environmental Protection Agency. Hence, it is essential to develop technologies to remediate FLT-contaminated groundwater and soil.

In recent years, advanced oxidation processes (AOPs) have raised significant interest due to their excellent ability to degrade massive amounts of hazardous organic pollutants in contaminated groundwater (Dong *et al.* 2018; Lai *et al.* 2019). Percarbonate (SPC), persulfate (PS), and hydrogen peroxide (H_2O_2) are often employed as oxidants in AOPs; among them, PS is favorable in groundwater remediation practice owing to the merits of longer half-life, high redox potential, convenient transportation and storage, broadly suitable pH range, etc. (Ghanbari & Moradi. 2017; Wu *et al.* 2022). Fe-based catalysts, particularly Fe(II), are commonly used as activators for PS because they are inexpensive, highly efficient, nontoxic, and widely available (El Asmar *et al.* 2021). The O–O bond in the PS structure is broken by Fe(II) activation and generates $SO_4^{-}\cdot$ which can be subsequently converted to HO• (Equations (1) and (2)) (Zhou *et al.* 2021).

$$S_2O_8^{2-} + Fe(II) \rightarrow Fe(III) + SO_4^{2-} + SO_4^{-}\bullet \quad (1)$$

$$H_2O + SO_4^{-}\bullet \rightarrow SO_4^{2-} + H^+ + HO\bullet \quad (2)$$

However, it is noted that PS activated by Fe(II) is insufficient due to the excessively rapid conversion of Fe(II) to Fe(III), which can interfere with the yield of $SO_4^{-}\cdot$ and HO• and further inhibit contaminant removal. Therefore, to increase the available dissolved Fe(II) concentration in the reaction, some researchers have proposed the heterogeneous catalytic process. Xu *et al.* (2021a) achieved 99.5% trichloroethylene removal in the PS/Fe(II)/nano zero-valent iron (nZVI) process with the presence of 1.0 critical micelle concentration (CMC) of Tween-80 (TW-80). Song *et al.* (2019) studied the effect of several types of nZVI on the removal of PAHs for PS activation in practical applications, and the results showed that the best PAH degradation was 82.2%. The excellent activation performance of nZVI for PS is because nZVI can accelerate the Fe(II)/Fe(III) cycle, which can bring about a high Fe(II) level in reaction and thus produce more reactive oxygen species (ROS) (Equation

(3)) (Xu *et al.* 2021a, 2021b). Nevertheless, given the high surface energy and magnetic interaction of nZVI particles, it has an aggregation propensity and tends to form iron hydroxides or iron oxides (Liang *et al.* 2021).

$$2Fe(III) + nZVI \rightarrow 3Fe(II) \quad (3)$$

In recent years, researchers have found that sulfidated nano zero-valent iron (S-nZVI) has higher catalytic reactivity and selectivity than nZVI (Zhou *et al.* 2021). The presence of an iron sulfide layer on S-nZVI is reported to eliminate hydrolysis reactions at the nVZI surface, which can boost the electron transfer efficiency from S-nZVI to target pollutants (Guo *et al.* 2010). Moreover, S(-II) also can act as a reductant in the Fe(II)/Fe(III) cycle (Equations (4)–(9)).

$$S(-II) + Fe(II) \rightarrow FeS \quad (4)$$

$$H^+ + FeS \rightarrow HS^- + Fe(II) \quad (5)$$

$$HS^- + 2Fe(III) \rightarrow S(0) + 2Fe(II) + H^+ \quad (6)$$

$$S(-II) + 2Fe(III) \rightarrow S(0) + 2Fe(II) \quad (7)$$

$$S(-II) + 8Fe(III) + 4H_2O \rightarrow SO_4^{2-} + 8Fe(II) + 8H^+ \quad (8)$$

$$S(0) + 6Fe(III) + 4H_2O \rightarrow SO_4^{2-} + 6Fe(II) + 8H^+ \quad (9)$$

Although S-nZVI is known to have been used in AOPs, FLT degradation in PS oxidation activated by S-nZVI as a catalyst has not been reported yet. In addition, the FLT degradation mechanism in the PS/S-nZVI system needs to be clarified to prevent the potential of secondary pollution. Therefore, this work was conducted to (1) examine FLT degradation efficiency in the PS/S-nZVI system and confirm the influence of chemical dosages on FLT degradation; (2) reveal the influence of water matrix on FLT removal; (3) elucidate the primary ROS in the PS/S-nZVI system and the activation mechanism for FLT degradation; (4) evaluate the practical performance of the PS/S-nZVI system for FLT removal in actual groundwater; (5) investigate the broad-spectrum reactivity of the system for other PAHs degradation; and finally, (6) propose the possible FLT degradation pathway in the PS/S-nZVI system.

2. MATERIALS AND METHODS

2.1. Materials and analytical methods

Details of the used materials and analytical methods in this research can be found in Text S1 and S2. Actual groundwater used in this test was obtained from a well screened 15-m-deep below the surface in Songjiang (Shanghai, China) with the main characteristics as shown in Table S3.

2.2. Experimental procedures

Batch experiments for FLT degradation in aqueous solution were conducted in a 250 mL cylindrical glass reactor with a magnetic stirring bar in it to ensure even distribution of all reagents throughout the reaction (600 rpm). The initial solution pH was not adjusted unless otherwise stated. All tests were maintained at a constant temperature of 20 ± 0.5 °C by a thermostatic water bath (DC, Ningbo, China).

The FLT concentration was set at 0.001 mM (0.2 mg L^{-1}) according to the reports and the US Environmental Protection Agency (EPA) DSSTox database (Ogbuagu *et al.* 2011). The pre-determined doses of S-nZVI and PS were added to the reactor containing 250 mL 0.001 mM FLT solution to start the reaction process, and the FLT concentration was set according to the solubility of FLT (0.26 mg L^{-1}). The amount of 0.7 mL sample was taken from the reactor and mixed with 0.7 mL methanol to terminate the reaction and then filtered for high-performance liquid chromatography (HPLC) analysis. The initial solution pH was adjusted by 0.1 M NaOH or 0.1 M H_2SO_4 in the experiment when investigating the effect of pH on FLT degradation.

In scavenging tests, scavengers were added to the reactor containing FLT solution before PS and S-nZVI addition. Experiments regarding the effects of groundwater matrix were carried out by initially adding $NaHCO_3$, NaCl, $NaNO_3$, Na_3PO_4, or humic acid (HA) into the reactor containing FLT solution, followed by the addition of other chemicals. Surfactants (triton X (TX-100), sodium dodecyl sulfate (SDS), polyoxyethylene lauryl ether (Brij-35), or TW-80) were added first, followed by other

reagents in experiments when exploring the influence of surfactants on FLT removal. All tests were conducted at least in triplicate and the mean values were reported.

3. RESULTS AND DISCUSSION

3.1. Effect of chemical doses on FLT degradation

The effect of PS and S-nZVI doses on FLT degradation was conducted in the PS/S-nZVI system. First, S-nZVI was set at 0.0072 g L^{-1} while PS varied from 0 to 0.14 mM. As shown in Figure 1(a), 4.9% FLT was lost in the blank test, showing

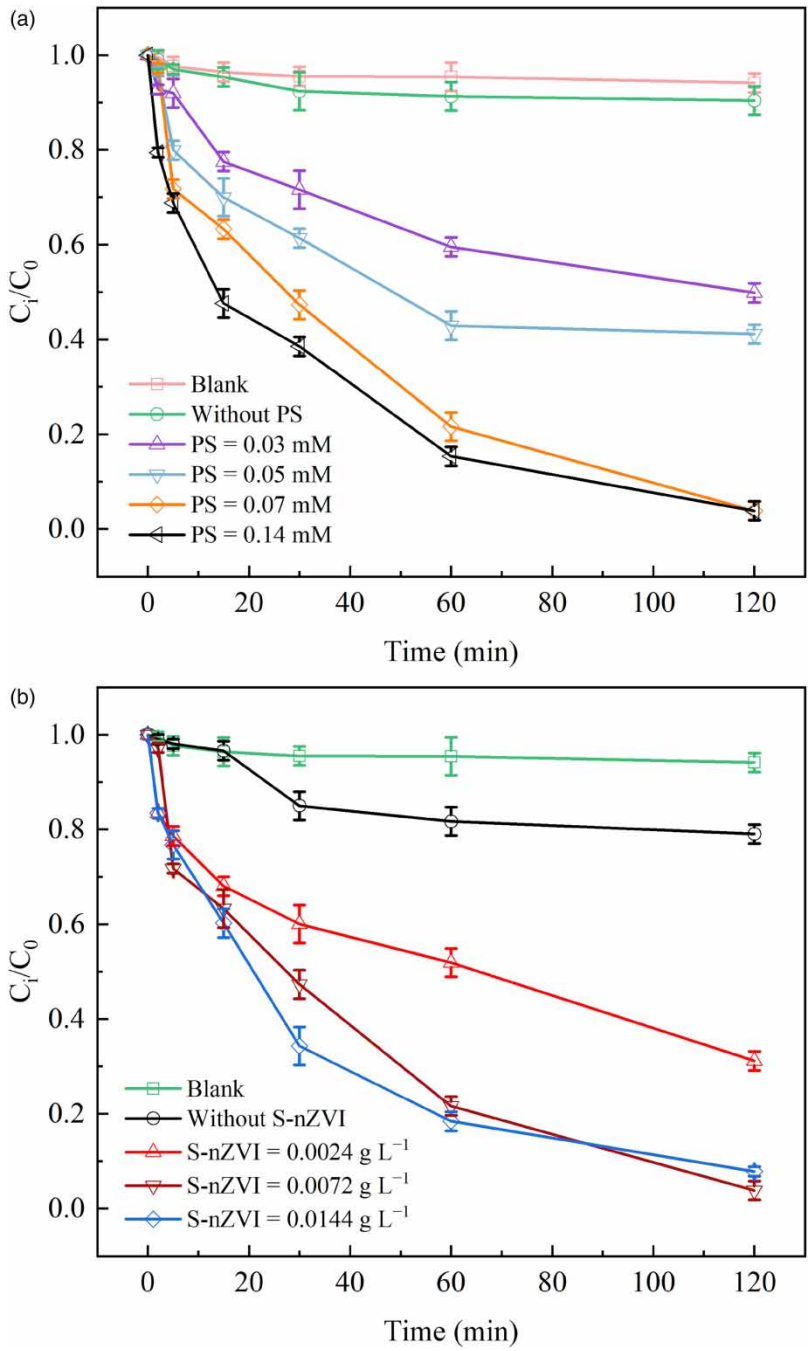

Figure 1 | Effect of (a) PS dose ($[S\text{-}nZVI]_0 = 0.0072$ g L^{-1}, $[FLT]_0 = 0.001$ mM) and (b) S-nZVI dose ($[PS]_0 = 0.07$ mM, $[FLT]_0 = 0.001$ mM) on FLT degradation.

that FLT volatilization could be neglected throughout the entire experiment. When only S-nZVI was added, the degradation of FLT was less than 10%, indicating that almost no direct reaction between S-nZVI and FLT occurred. FLT degradation was significantly higher as the concentration of PS increased from 0.03 to 0.07 mM, confirming that an appropriate increase in PS dose could generate more ROS. However, when the PS dose was further increased to 0.14 mM, there was almost no change in FLT removal. The reason for this phenomenon could be that $SO_4^-\cdot$ concentration was elevated with the increase in PS dose and then might have reacted with HO•, $S_2O_8^{2-}$, and $SO_4^-\cdot$ when $SO_4^-\cdot$ was in excess, leading to self-loss of the available ROS (Equations (10)–(12)). Hence, 0.07 mM was selected as the optimal dose of PS based on the removal performance of FLT and economic consideration.

$$SO_4^-\bullet + S_2O_8^{2-} \rightarrow SO_4^{2-} + S_2O_8^-\bullet \quad (10)$$

$$SO_4^-\bullet + SO_4^-\bullet \rightarrow S_2O_8^{2-} \quad (11)$$

$$SO_4^-\bullet + HO\bullet \rightarrow HSO_4^- + 1/2O_2 \quad (12)$$

Second, the dose of S-nZVI was varied to investigate its effect on FLT degradation while PS concentration was set at 0.07 mM. As shown in Figure 1(b), only 20% FLT was degraded when only PS was added, demonstrating that the reaction of PS alone with FLT was very slow. However, FLT degradation increased to 69.9 and 96.2% as S-nZVI was increased to 0.0024 and 0.0072 g L^{-1}, respectively. When the S-nZVI dose was further raised to 0.0144 g L^{-1}, FLT degradation slightly decreased, showing that FLT degradation would not rise indefinitely with the increase in S-nZVI dose. This behavior could be caused by the reaction between the generated ROS and S-nZVI, and ROS became depleted when S-nZVI was in excess. Therefore, the following experiments were conducted at the optimal dosage conditions for PS and S-nZVI, which were set at 0.07 mM and 0.0072 g L^{-1}, respectively.

To further validate the synergistic effect of PS and S-nZVI on FLT removal, the synergistic index (Q) of FLT removal was calculated. Here, E_{a+b} is FLT removal with PS and S-nZVI effects together, E_a is FLT removal with the PS effect alone, and E_b is FLT removal with the S-nZVI effect alone (Equation (13)). Meanwhile, $Q < 0.85$ is antagonistic, $0.85 \leq Q < 1.15$ is additive, and $Q \geq 1.15$ is synergistic. After calculation in this research, the yielded $Q = 3.36 > 1.15$; thus, the synergistic effect for FLT removal by PS and S-nZVI was confirmed.

$$Q = \frac{E_{a+b}}{E_a + E_b - E_a \times E_b} \quad (13)$$

As presented in Fig. S1a, the maximum total Fe concentration during the reaction was less than 0.012 mM (0.67 mg L^{-1}), and the concentration of total Fe in the standard for groundwater quality (IV Class, GB/T 14848-2017 China) is 2.0 mg L^{-1}, suggesting that the Fe ion concentration generated in the experiment meets the standard for groundwater quality (IV Class, GB/T 14848-2017 China). The SO_4^{2-} concentration during the reaction was identified (Fig. S1b), and the maximum SO_4^{2-} was 7.68 mg L^{-1}, while the concentration of SO_4^{2-} in the standard for groundwater quality (IV Class, GB/T 14848-2017 China) was 350 mg L^{-1}, indicating that the SO_4^{2-} concentration generated in the experiment also meets the standard for groundwater quality (IV Class, GB/T 14848-2017 China).

3.2. Mechanisms of FLT degradation in PS/S-nZVI system

3.2.1. Characterization of S-nZVI

In order to improve the dispersion properties, stability, and electron selectivity of nZVI particles, the surface of nZVI particles was vulcanized to form S-nZVI, which means that the surface of S-nZVI particles is FeS, and nZVI particles are encapsulated in core by FeS. S-nZVI before and after the reaction were characterized by scanning electron microscopy (SEM) and energy-dispersive spectroscopy (EDS). As shown in Figure 2(a) and 2(b), fresh S-nZVI were lamellar and the spent S-nZVI particles were spherical, indicating the full participation of S-nZVI in the reaction. The S-nZVI surface was quite rough due to the presence of the FeS layer. Furthermore, S-nZVI did not aggregate significantly after the reaction because of its hydrophobicity property which was different from nZVI (Fan *et al.* 2017). Five S-nZVI particles with uniform particle size were selected to determine the average particle size of S-nZVI, which was calculated to be about 0.12 nm (Figure 2(b)). The EDS results showed that Fe and S contents decreased from 87.22 and 1.99% to 79.74 and 1.08%, respectively, while O content increased

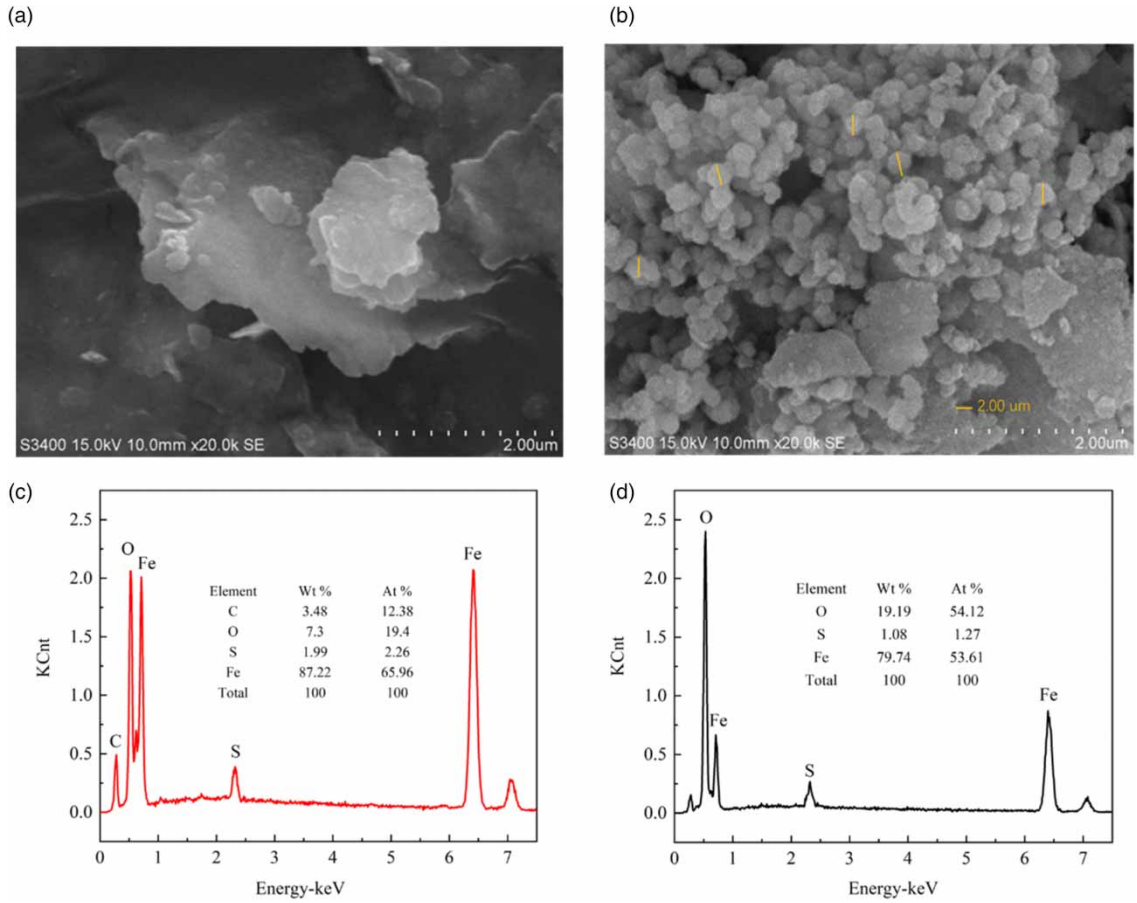

Figure 2 | SEM images of (a) fresh S-nZVI particles and (b) spent S-nZVI particles, and EDS spectra of (c) fresh S-nZVI particles and (d) spent S-nZVI particles.

from 7.3 to 19.19% accordingly (Figure 2(c) and 2(d)). The decrease in Fe content was from the FeS layer on the surface and the internal nZVI particles, the decrease in S content was due to the FeS layer, and the increase in O content was due to the oxidation of nZVI inside S-nZVI particles. This phenomenon again suggested that there was an oxidation reaction taking place on the S-nZVI surface, which was consistent with the SEM results.

The X-ray diffraction (XRD) patterns of S-nZVI before and after the reaction are shown in Fig. S2. The typical peaks at 2θ values of 44.68° and 65.04° corresponded to the planes (110) and (200) of α-Fe^0 (JCPDS No. 06-0696) (Zhou *et al.* 2021). The peak at 44.68° before the reaction was much higher than the peak at 65.04°, suggesting that the plane (110) of α-Fe^0 in S-nZVI particles was larger than the plane (200). After the reaction, the Fe^0 peak in S-nZVI particles was attenuated. However, no significant FeS peaks were detected, which could be attributed to the low content of FeS. Transmission electron microscope (TEM) analysis of fresh S-nZVI particles showed that these particles have a distinct granular structure (Figure 3(a)). As presented in Figure 3(b), a clear lattice fringe of 0.26 nm was exhibited, which was well indexed to the (110) crystal plane of Fe^0 particles. In addition, the clear lattice fringe corresponding to the (200) plane of Fe^0 was absent, probably due to the fact that the lattice plane (110) was the main exposed surface, which was consistent with the XRD results. The functional groups and chemical bonds of S-nZVI detected by a Fourier transform infrared spectrometer (FTIR) spectrum changed significantly before and after the reaction (Fig. S3). Significant Fe–O and O–H vibrations were observed at 588.8 and 3336.4 cm^{-1} in S-nZVI (Liu *et al.* 2017; Zhou *et al.* 2021). S–O vibrations were reported to be around 1120 cm^{-1}, but the vibrations at 1120 cm^{-1} were not obvious in Fig. S3, which might be due to the low S content of S-nZVI used in the experiment.

The valence changes of the surface elements of S-nZVI before and after the reaction were analyzed using X-ray photoelectron spectroscopy (XPS) analysis. In Figure 4(a), the Fe 2p peaks at 710.1 eV and 711.0 were assigned to Fe $2p_{1/2}$ for Fe(II) and Fe(III), respectively. The peaks at 724.0 and 726.2 eV corresponded to Fe $2p_{3/2}$ of Fe(II) and Fe(III), respectively

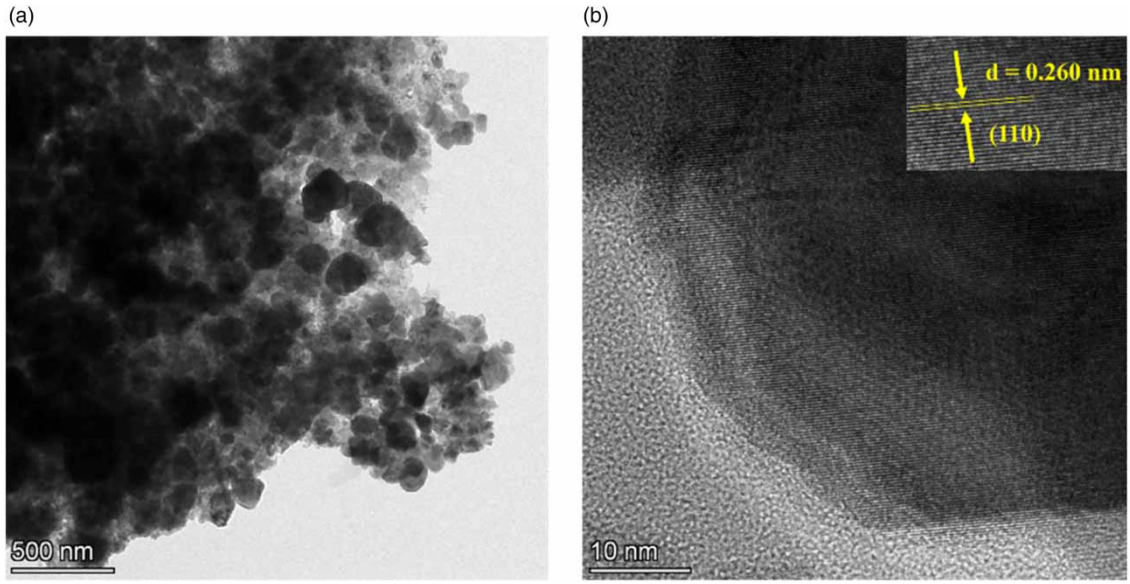

Figure 3 | TEM images of fresh S-nZVI, (a) 500 nm scale and (b) 10 nm scale.

(Figure 4(b)) (Du *et al.* 2016; Xu *et al.* 2021a, 2021b). The peak of Fe on the surface of S-nZVI changed significantly after the reaction compared to that before the reaction, validating the valence and morphological transformation of Fe in the reaction. The S 2p spectrum of fresh S-nZVI showed two peaks at 163.4 and 168.5 eV, attributed to FeS and surface-bound SO_4^{2-}, respectively (Figure 4(c)). The S 2p spectra of the spent S-nZVI showed three curves at 162.8, 168.0, and 169.0 eV, corresponding to FeS, SO_4^{2-}, and SO_4^{2-}groups, respectively (Du *et al.* 2016; Xu *et al.* 2021a, 2021b). It is noteworthy that the FeS content of the S-nZVI surface significantly reduced and SO_4^{2-} content increased after the reaction compared to those before the reaction, verifying the valence and morphological transformation of S before and after use (Equations (7)–(9)).

3.2.2. ROS identification

According to the reports, several ROS are generated in the system with PS as an oxidant and may also be produced in the PS/S-nZVI system (Yu *et al.* 2018). Thus, three probe compounds, namely nitrobenzene (NB), carbon tetrachloride (CT), and anisole (AN), were used to identify ROS generated in the PS/S-nZVI system. Information about the probe compounds is listed in Text S3. All three compounds showed varying degrees of degradation as shown in Fig. S4, which demonstrated the presence of HO•, O_2^-•, and SO_4^-• in the PS/S-nZVI system. Since there was no suitable $^1O_2$ probe, an electron paramagnetic resonance (EPR) test was conducted to confirm the presence of $^1O_2$ (Entradas *et al.* 2020).

ROS generated in the PS/S-nZVI system was further determined by EPR detection with 5,5-dimethyl-1-oxypyrrolidine (DMPO) and 2,2,6,6-tetramethylpiperidine (TEMP) as trapping reagents. As illustrated in Figure 5(a) and 5(b), the signals of DMPO-HO•, DMPO-SO_4^-•, and TEMP-$^1O_2$ adducts suggested that HO•, SO_4^-•, and $^1O_2$ were generated in the PS/S-nZVI system. Unfortunately, no adducts of DMPO with O_2^-• were detected due to its rapid conversion to $^1O_2$ and low concentration (Equation (14)).

$$O_2^-\bullet + HO\bullet \rightarrow {}^1O_2 + OH^- \tag{14}$$

Moreover, scavenging experiments were carried out to confirm the extent of the influence of ROS on FLT degradation. Four scavengers, namely tert-butyl alcohol (TBA), isopropanol (IPA), chloroform (CF), and furfuryl alcohol (FFA), were used in these tests and their characteristics are listed in Text S3. As shown in Figure 5(c), FLT degradation decreased from 96.2 to 68.4% when TBA (a scavenger of HO•) was added, indicating the important role of HO• in FLT removal. In addition, FLT degradation was severely suppressed with the addition of excess IPA (scavenger of HO• and SO_4^-•), confirming that SO_4^-• also had a significant contribution to FLT degradation. Compared with the inhibition by TBA, FLT degradation was around 20% with the addition of FFA (HO• and $^1O_2$ scavenger), which demonstrated the indelible contribution of

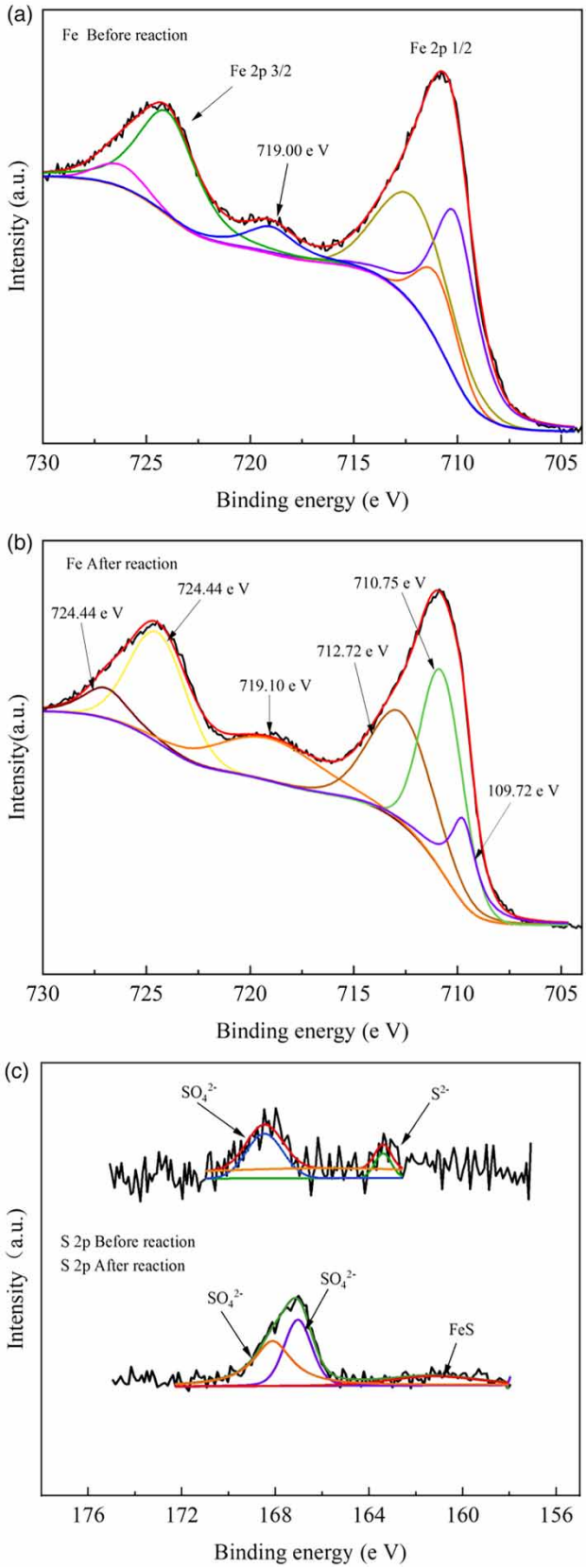

Figure 4 | XPS spectra of Fe 2p region of (a) fresh S-nZVI and (b) spent S-nZVI, and (c) S 2p region of the fresh and spent S-nZVI.

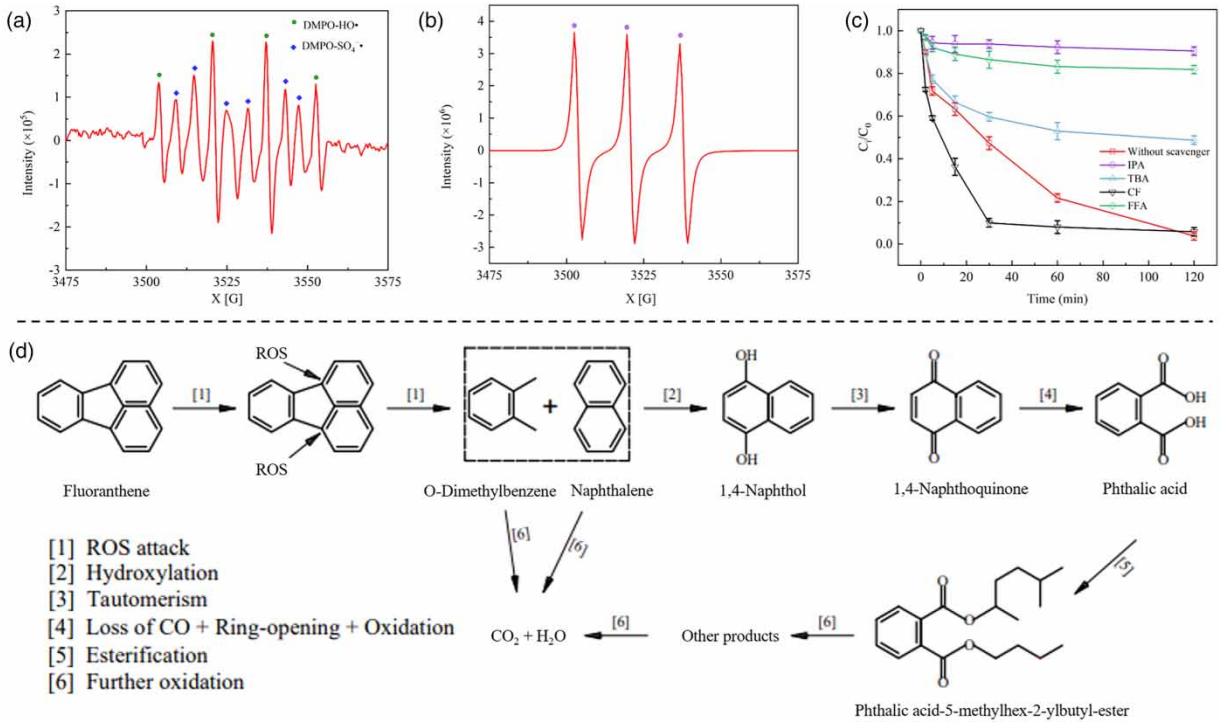

Figure 5 | EPR spectrum at the reaction time of 10 min in the PS/S-nZVI system with (a) DMPO as a trapper and (b) TEMP as a trapper, (c) effect of scavengers on FLT degradation in the PS/S-nZVI system, and (d) proposed FLT degradation pathway in the PS/S-nZVI system. ($[IPA]_0 = [TBA]_0 = [CF]_0 = [FFA]_0 = 10$ mM, $[PS]_0 = 0.07$ mM, $[S\text{-}nZVI]_0 = 0.0072$ g L^{-1}, $[FLT]_0 = 0.001\,7$mM).

$^1O_2$ to FLT degradation as well. Since CF scavenged $O_2^-\bullet$ from the solution, the addition of CF prevented $O_2^-\bullet$ from reacting with HO•, ultimately facilitating the removal of FLT. It is worth noting that FLT degradation did not change significantly after the addition of CF, indicating that $O_2^-\bullet$ hardly contributed to FLT degradation in the PS/S-nZVI system.

In conclusion, both HO• and $SO_4^-\bullet$ were the major ROS in FLT degradation with HO• being more vital than $SO_4^-\bullet$. This was because of the conversion of $SO_4^-\bullet$ to HO• (Equation (2)), and some scholars had found that HO• converted from $SO_4^-\bullet$ played a greater role than $SO_4^-\bullet$ itself (Zhou *et al.* 2021).

3.2.3. FLT degradation pathway

The gas chromatograph-mass spectrometry (GC-MS) technology was used to identify FLT degradation intermediates in the PS/S-nZVI process. The GC-MS spectrogram, FLT degradation intermediates spectra, and information of the intermediates are shown in Fig. S5, Fig. S6, and Table S4, respectively.

In this study, *o*-xylene and naphthalene (NAP), two intermediates of FLT degradation, were detected, and the possible degradation pathway of FLT in the PS/S-nZVI system was hypothesized based on the above intermediates (Figure 5(d)). First, FLT was attacked by ROS (position indicated by arrows) to produce *o*-dimethylbenzene (*o*-xylene) and NAP. NAP was transformed to 1,4-naphthol by hydroxylation, which subsequently underwent tautomerization to 1,4-naphthoquinone. Then, 1,4-naphthoquinone was further oxidized to other small organic compounds, and finally, partially decomposed to H_2O and CO_2. In addition, *o*-xylene and NAP may be partially and directly decomposed to H_2O and CO_2.

3.3. Effect of different water matrix on FLT removal

3.3.1. Effect of the initial solution pH on FLT removal

The initial solution pH is known to play an important role in PS-based Fenton or Fenton-like reactions. Therefore, the influence of the initial solution pH on FLT removal in the PS/S-nZVI system was determined by pre-adjusting the solution pH to 3.0, 5.0, 7.0, 9.0, and 11.0 before PS addition. As can be seen from Figure 6(a) and Table 1, there was no significant change in FLT degradation when pH was 3.0 and 5.0, while FLT degradation plummeted to 48.2, 18.4, and 6.9% when pH increased to

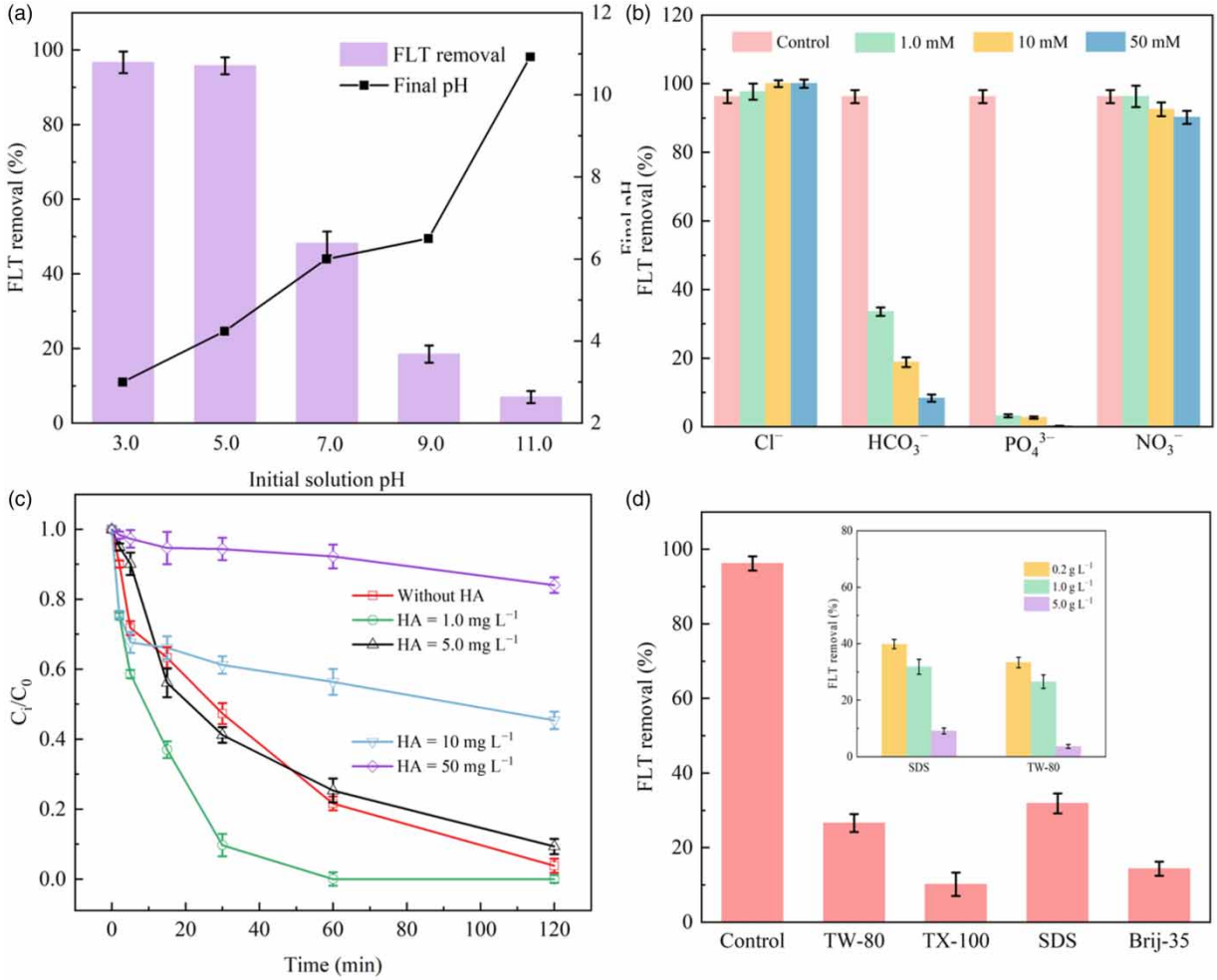

Figure 6 | Effects of (a) initial solution pH, (b) anions (Cl^-, HCO_3^-, PO_4^{3-}, and NO_3^-), (c) HA, and (d) surfactants ($[TW\text{-}80]_0 = [SDS]_0 = [TX\text{-}100]_0 = [Brij\text{-}35]_0 = 1.0\ g\ L^{-1}$) on FLT degradation in the PS/S-nZVI system. ($[PS]_0 = 0.07$ mM, $[S\text{-}nZVI]_0 = 0.0072\ g\ L^{-1}$, $[FLT]_0 = 0.001$ mM).

7.0, 9.0, and 11.0, respectively. The possible reasons for this phenomenon are as follows. First, FeS on the surface layer of S-nZVI was less susceptible to corrosion at pH greater than 7.0, so the dissolved Fe(II) was not sufficient to activate PS and it was susceptible to conversion to precipitation. Second, under an alkaline condition, $SO_4^-\bullet$ would convert to HO• which is less oxidizable in an alkaline environment (Equation (15)), leading to a decrease in FLT degradation. It is worth mentioning that SO_4^{2-} generated from PS also inhibited the activity of HO• to some degree (Liang *et al.* 2007). Based on the above results, it is concluded that an acidic condition was more beneficial to FLT degradation in the PS/S-nZVI process.

$$SO_4^-\bullet + OH^- \rightarrow HO\bullet + SO_4^{2-} \tag{15}$$

3.3.2. Effect of anions on FLT degradation

For a better investigation of the PS/S-nZVI system in practical situations, Table 2 and Figure 6(b) show the influence of anions, including Cl^-, HCO_3^-, PO_4^{3-}, and NO_3^- being prevalent in groundwater, on FLT degradation. To fully assess the behavior of different concentrations of anions, each anion was set to 1.0, 10, and 50 mM. It has been reported that Cl^- is a scavenger of HO• and generates low reactive radicals such as $Cl_2^-\bullet$ during the reaction, which can negatively affect FLT degradation (Equations (16)–(18)) (Yang *et al.* 2021). However, FLT degradation in this study with the presence of Cl^- did not decrease but slightly increased, which was completely contrary to the above report. This phenomenon can be explained by the following reasons. According to Equations (19)–(21), HO• was regenerated by the transformation of Cl• and $Cl_2^-\bullet$ and

Table 1 | Parameter values in the PS/S-nZVI system

Experimental conditions	pH (initial/final)	FLT removal (%)
PS = 0.07 mM, [S-nZVI] = 0.072 g L^{-1}, pH unadjusted	5.85/4.52	96.2
pH = 3.0	3.04/3.01	96.7
pH = 5.0	4.96/4.25	96.8
pH = 7.0	7.07/6.01	48.2
pH = 9.0	8.99/6.51	18.5
pH = 11.0	10.98/10.94	7.0
[a]PS = 0.07 mM, [S-nZVI] = 0.072 g L^{-1}	7.76/7.85	2.1
[a]PS = 0.42 mM, [S-nZVI] = 0.432 g L^{-1}	7.95/7.90	6.4
[a]PS = 0.21 mM, [S-nZVI] = 0.216 g L^{-1}	7.78/7.84	5.1
[a]PS = 0.35 mM, [S-nZVI] = 0.360 g L^{-1}	7.76/7.76	6.8
[a]PS = 0.07 mM, [S-nZVI] = 0.072 g L^{-1}	4.01/3.97	16.1
[b]pH = 4.0		
[a]PS = 0.21 mM, [S-nZVI] = 0.216 g L^{-1}	4.05/3.55	33.9
[b]pH = 4.0		
[a]PS = 0.35 mM, [S-nZVI] = 0.360 g L^{-1}	3.98/3.54	79.4
[b]pH = 4.0		
[a]PS = 0.42 mM, [S-nZVI] = 0.432 g L^{-1}	4.06/3.41	86.4
[b]pH = 4.0		

[a]Experiments were conducted by using actual groundwater.
[b]pH was pre-adjusted to 4.0.

Table 2 | Parameter values for testing the effect of water matrix on FLT degradation

Experimental conditions	PS/S-nZVI	pH (initial/final)	FLT removal (%)
Cl^- = 1.0 mM	PS = 0.07 mM, [S-nZVI] = 0.072 g L^{-1}	5.91/4.76	97.7
Cl^- = 10 mM		5.82/4.26	100
Cl^- = 50 mM		5.88/4.06	100
HCO_3^- = 1.0 mM		8.16/7.92	33.6
PO_4^{3-} = 50 mM		12.99/12.98	0.3
NO_3^- = 1.0 mM		8.62/8.61	8.3
HCO_3^- = 10 mM		8.67/8.66	18.8
HCO_3^- = 50 mM		6.18/4.08	97.3
NO_3^- = 10 mM		6.11/4.62	90.5
NO_3^- = 50 mM		6.15/4.84	90.2
PO_4^{3-} = 1.0 mM		11.13/11.10	3.2
PO_4^{3-} = 10 mM		11.92/11.90	2.7
HA = 1.0 mg L^{-1}	PS = 0.07 mM, [S-nZVI] = 0.072 g L^{-1}	5.98/4.06	100
HA = 5.0 mg L^{-1}		5.72/4.43	90.1
HA = 10 mg L^{-1}		5.85/4.32	54.6
HA = 50 mg L^{-1}		6.48/5.94	15.9
HA = 100 mg L^{-1}		7.02/6.51	4.1

the decomposition of $ClHO^{-}\bullet$, which could mitigate the self-scavenging of HO• by lowering the HO• concentration in solution to some extent, thus the presence of Cl^{-} facilitated FLT removal (Wang & Wang 2020).

$$HO\bullet + Cl^{-} \rightarrow ClHO^{-}\bullet \quad (16)$$

$$ClHO^{-}\bullet + H^{+} \rightarrow Cl\bullet + H_2O \quad (17)$$

$$Cl\bullet + Cl^{-} \rightarrow Cl_2^{-}\bullet \quad (18)$$

$$Cl\bullet + H_2O \rightarrow HCl + HO\bullet \quad (19)$$

$$Cl_2^{-}\bullet + H_2O \rightarrow 2Cl^{-} + HO\bullet + H^{+} \quad (20)$$

$$ClHO^{-}\bullet \rightarrow Cl^{-} + HO\bullet \quad (21)$$

The influence of NO_3^{-} on FLT degradation was insignificant, and the degradation of FLT could reach more than 90% even at 50 mM of NO_3^{-}. However, both HCO_3^{-} and PO_4^{3-} significantly inhibited FLT degradation. The reasons were as follows:

(1) Both HCO_3^{-} and PO_4^{3-} could dramatically increase the initial solution pH, which had an inhibitory effect on FLT degradation.
(2) HCO_3^{-} and PO_4^{3-} could generate basic buffer pairs, such as CO_3^{2-}/HCO_3^{-} and HPO_4^{2-}/PO_4^{3-}, which could fail to keep FLT degradation in the PS/S-nZVI system in an ideal acidic environment (Liu *et al.* 2021).
(3) HCO_3^{-} could react with HO• and $SO_4^{-}\bullet$ to form less reactive $HCO_3\bullet$ (Equations (22) and (23)) which was not conducive to FLT degradation (Wu & Linden 2010).

$$HCO_3^{-} + HO\bullet \rightarrow OH^{-} + HCO_3\bullet \quad (22)$$

$$HCO_3^{-} + SO_4^{-}\bullet \rightarrow SO_4^{2-} + HCO_3\bullet \quad (23)$$

In addition, Diao *et al.* (2020) reported that NO_3^{-} and SO_4^{2-} had no significant influence on the target pollutant's degradation, in studies using PS as an oxidant for the degradation of organic pollutants. The results of NO_3^{-} were similar to this experiment. Moreover, the dose of PS was only 0.07 mM, so the amount of SO_4^{2-} produced by the decomposition of PS was not large enough to affect FLT removal.

3.3.3. Effect of HA on FLT removal

Given that HA is an important part of natural organic matter (NOM) which is widely present in groundwater, it is chosen as a representative of NOM to investigate its influence on FLT removal in the PS/S-nZVI process. From Figure 6(c) and Table 2, it can be seen that HA accelerated FLT degradation when the HA concentration was set as 1.0 mg L^{-1}. This result can be explained by the following reasons. HA can complex with Fe(III) to prevent iron precipitation to some extent, while Fe(0), S(-II), and S(0) can act as reductants of Fe(III) to promote the regeneration of Fe(II), which ensures the long-term activation of PS and ultimately raises the concentration of $SO_4^{-}\cdot$ and HO• in the PS/S-nZVI system (Georgi *et al.* 2007; Wang *et al.* 2016). What is more, it has been found that 1.0 mg L^{-1} HA could increase the amount of HO• in AOPs (Sheng & Lyu 2023). However, HA can compete with FLT for HO• since it is an organic substance, and the competition of HA for HO• is dominant in the PS/S-nZVI system at a higher concentration of HA.

3.3.4. Effect of surfactants on FLT removal

Surfactants are widely used because they can increase pollutants' solubility by reducing surface tension, therefore, desorbing pollutants from soil medium into aqueous solution (Mao *et al.* 2015). Nevertheless, the presence of surfactants can influence the degradation of contaminants in AOPs. Therefore, the influence of TX-100, SDS, Brij-35, and TW-80 as surfactant representatives on FLT degradation in the PS/S-nZVI system was explored and Table S1 shows their characteristics. Considering the high concentration of surfactant (1.0–20 g L^{-1}) used in practical applications and the limited chemical amount applied in this work, the concentration of different surfactants was set at 1.0 g L^{-1} in the present experiment (Dugan *et al.* 2010).

As shown in Figure 6(d), FLT removal was substantially inhibited in the presence of surfactants with the highest degradation being only 31.8% in the presence of SDS. First, surfactants are a kind of organic substance that could compete with FLT for ROS and thus inhibit FLT degradation (García-Cervilla *et al.* 2021). Similarly, in the research of trichloroethene

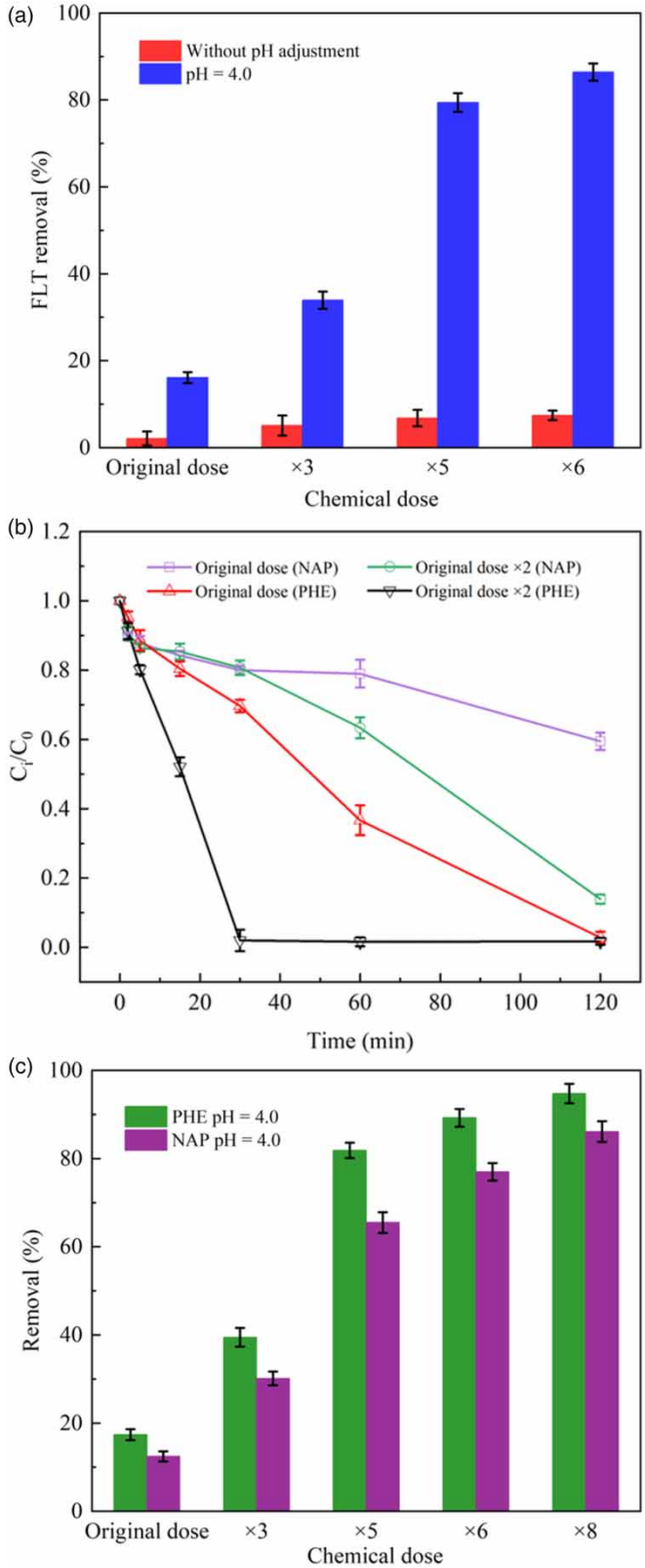

Figure 7 | (a) FLT degradation performance in actual groundwater in the PS/S-nZVI system, and the broad-spectrum reactivity of the PS/S-nZVI process in remediation of NAP and PHE in (b) ultrapure water and (c) actual groundwater. ($[NAP]_0 = 0.02$ mM, $[PHE]_0 = 1.0$ mg L^{-1}, original $[PS]_0 = 0.07$ mM, original $[S\text{-}nZVI]_0 = 0.0072$ g L^{-1}).

(TCE) degradation by PS as an oxidant, it was found by EPR that TW-80, TX-100, and Brij-35 could inhibit TCE degradation through HO• depletion (Sun *et al.* 2021). Second, when the concentration of surfactants was more than the CMC, surfactant micelles were voluntarily generated and encapsulated the FLT molecules in the micelle core, so the ROS needed to disrupt the micelles before reacting with FLT (Wang *et al.* 2017). Furthermore, SDS and TW-80, currently popular representatives of anionic and nonionic surfactants, were studied for their influences on FLT degradation at different concentrations (Figure 6(d) insert). The results, not surprisingly, showed that FLT removal decreased with increasing surfactant concentration, where TW-80 inhibited more significantly than SDS which was probably because TW-80 has a much smaller CMC than SDS, thus more micelles were generated that required more ROS to disrupt.

3.4. FLT degradation in actual groundwater remediation

To further explore FLT degradation by the PS/S-nZVI process in practice, actual groundwater was used to substitute ultrapure water for simulation. Table S2 shows the main parameters of actual groundwater. According to Figure 7(a) and Table 1, FLT was barely degraded (2.1%) at PS and S-nZVI doses of 0.07 mM and 0.0072 g L^{-1}, respectively, which was significantly lower than the result obtained from the ultrapure water system (96.2%). This mainly contributed to the relatively high initial solution pH (7.9) and high buffering capacity, the presence of NOM, and the high concentration of HCO_3^- (191.3 mg L^{-1}). Nevertheless, FLT removal (7.4%) was also not satisfactory when PS and S-nZVI doses were increased to six folds than the initial doses. To our delight, FLT removal was significantly enhanced by pre-adjusting the initial solution pH to 4.0 with FLT degradation up to 86.4% at six folds of the initial doses. This result demonstrated that the PS/S-nZVI system was suitable for actual groundwater remediation contaminated by FLT after the pre-adjustment of pH.

3.5. The broad applicability of PS/S-nZVI process

In actual contaminated groundwater with PAHs, NAP and phenanthrene (PHE) are also usually present along with FLT. Therefore, to further verify the superiority of this technique, NAP and PHE were investigated to demonstrate the broad applicability of the PS/S-nZVI process. The initial concentrations of NAP and PHE were set at 0.02 and 0.005 mM, respectively.

In Figure 7(b), PHE degradation reached 97.2% at the initial chemical doses, while NAP was also degraded up to 86% when the doses doubled. Even at actual groundwater conditions, PHE and NAP were able to be degraded to 94.7 and 86.1%, respectively, after the chemical doses were increased eight folds when the pH was pre-adjusted to 4.0 (Figure 7(b) and 7(c)). This could be due to HO• and $SO_4^{-\bullet}$ produced in the PS/S-nZVI system, which is also effective in PHE and NAP degradation (Yu *et al.* 2018; Zeng *et al.* 2022). In conclusion, the above results confirmed that besides FLT, the PS/S-nZVI process could also degrade the other two common PAHs, strongly demonstrating its excellence in PAH contaminated groundwater remediation.

3.6. The reusability and long-term stability of S-nZVI

S-nZVI was reused three times under the same condition and the results are shown in Fig. S7. The catalytic performance of S-nZVI after three cycles decreased by 58.0%, indicating that S-nZVI exhibited some reusable properties to some extent. Besides, XRD analysis of the fresh and used S-nZVI showed that the initial crystal structure of S-nZVI was preserved, which further confirmed its certain structural stability (Fig. S2). Therefore, S-nZVI has a certain stability and reusability, which is favorable for practical applications.

4. CONCLUSIONS

In this work, 96.3% of FLT could be removed within 120 min in the PS/S-nZVI system when the doses of PS and S-nZVI were 0.07 mM and 0.0072 g L^{-1}, respectively. HO• and $SO_4^{-}\cdot$ were the critical ROS in FLT degradation in the PS/S-nZVI system. S-nZVI could effectively accelerate the Fe(II)/Fe(III) cycle, in which sulfur species acted as a reductant to some extent. FLT removal in the PS/S-nZVI system was favorable under acidic conditions, and HCO_3^-, PO_4^{3-}, and surfactants inhibited the degradation of FLT. Cl^- slightly promoted FLT degradation while NO_3^- had no significant effect on it. FLT degradation could be accelerated at 1.0 mg L^{-1} HA presence but inhibited when the HA concentration increased. Based on the detected intermediates *o*-xylene and NAP, a degradation pathway for FLT was proposed. By pre-adjusting the solution pH to 4.0 and increasing the chemical doses to 6-fold the original one, the PS/S-nZVI process was able to degrade 86.4% of FLT in actual groundwater. Finally, the PS/S-nZVI process also showed an outstanding performance in the removal of NAP and PHE, displaying a great prospect of this technique in the remediation of PAHs-contaminated groundwater.

ACKNOWLEDGEMENTS

We are sincerely grateful to the reviewers and the editor for their useful comments that have helped us to improve the quality of our study.

AUTHOR CONTRIBUTIONS

All authors contributed to the study's conception and design. R. Z., Y. Z., and J. D. wrote the main manuscript text. Z. Y. and G. Z. prepared all the figures. X. S. and Z. X. prepared all the tables. S. L. was responsible for validation and supervision. All authors reviewed the manuscript. All authors read and approved the final manuscript.

FUNDING

This study was financially sponsored by the Shanghai Rising-Star Program (No. 22QB1401700).

CONSENT TO PARTICIPATE

All authors mentioned in this paper agreed to participate in this study.

CONSENT FOR PUBLICATION

If the manuscript is accepted, the authors mentioned in this study agree to publish the paper.

DATA AVAILABILITY STATEMENT

All relevant data are included in the paper or its Supplementary Information.

CONFLICT OF INTEREST

The authors declare there is no conflict.

REFERENCES

Diao, Z. H., Dong, F. X., Yan, L., Chen, Z. L., Qian, W., Kong, L. J., Zhang, Z. W., Zhang, T., Tao, X. Q., Du, J. J., Jiang, D. & Chu, W. 2020 Synergistic oxidation of Bisphenol A in a heterogeneous ultrasound-enhanced sludge biochar catalyst/persulfate process: Reactivity and mechanism. *Journal of Hazardous Materials* **384**, 121385.

Dong, C. D., Tsai, M. L., Chen, C. W. & Hung, C. M. 2018 Remediation and cytotoxicity study of polycyclic aromatic hydrocarbon-contaminated marine sediments using synthesized iron oxide–carbon composite. *Environmental Science and Pollution Research* **25** (6), 5243–5253.

Du, J., Bao, J., Lu, C. & Werner, D. 2016 Reductive sequestration of chromate by hierarchical FeS@Fe^0 particles. *Water Research* **102**, 73–81.

Dugan, P. J., Siegrist, R. L. & Crimi, M. L. 2010 Coupling surfactants/cosolvents with oxidants for enhanced DNAPL removal: A review. *Remediation Journal* **20** (3), 27–49.

El Asmar, R., Baalbaki, A., Abou Khalil, Z., Naim, S., Bejjani, A. & Ghauch, A. 2021 Iron-based metal organic framework MIL-88-A for the degradation of naproxen in water through persulfate activation. *Chemical Engineering Journal* **405**, 126701.

Entradas, T., Waldron, S. & Volk, M. 2020 The detection sensitivity of commonly used singlet oxygen probes in aqueous environments. *Journal of Photochemistry and Photobiology B: Biology* **204**, 111787.

Fan, D., Lan, Y., Tratnyek, P. G., Johnson, R. L., Filip, J., O'Carroll, D. M., Garcia, A. & Agrawal, A. 2017 Sulfidation of iron-based materials: A review of processes and implications for water treatment and remediation. *Environmental Science & Technology* **51** (22), 13070–13085.

García-Cervilla, R., Santos, A., Romero, A. & Lorenzo, D. 2021 Compatibility of nonionic and anionic surfactants with persulfate activated by alkali in the abatement of chlorinated organic compounds in aqueous phase. *Science of the Total Environment* **751**, 141782.

Georgi, A., Schierz, A., Trommler, U., Horwitz, C. P., Collins, T. J. & Kopinke, F. D. 2007 Humic acid modified Fenton reagent for enhancement of the working pH range. *Applied Catalysis B: Environmental* **72** (1–2), 26–36.

Ghanbari, F. & Moradi, M. 2017 Application of peroxymonosulfate and its activation methods for degradation of environmental organic pollutants. *Chemical Engineering Journal* **310**, 41–62.

Guo, L., Chen, F., Fan, X., Cai, W. & Zhang, J. 2010 S-doped α-Fe_2O_3 as a highly active heterogeneous Fenton-like catalyst towards the degradation of acid orange 7 and phenol. *Applied Catalysis B: Environmental* **96** (1–2), 162–168.

Lai, C., Zhang, M., Li, B., Huang, D., Zeng, G., Qin, L., Liu, X., Yi, H., Cheng, M., Li, L., Chen, Z. & Chen, L. 2019 Fabrication of CuS/$BiVO_4$ (0 4 0) binary heterojunction photocatalysts with enhanced photocatalytic activity for Ciprofloxacin degradation and mechanism insight. *Chemical Engineering Journal* **358**, 891–902.

Liang, C., Wang, Z. S. & Bruell, C. J. 2007 Influence of pH on persulfate oxidation of TCE at ambient temperatures. *Chemosphere* **66** (1), 106–113.

Liang, L., Li, X., Guo, Y., Lin, Z., Su, X. & Liu, B. 2021 The removal of heavy metal cations by sulfidated nanoscale zero-valent iron (S-nZVI): The reaction mechanisms and the role of sulfur. *Journal of Hazardous Materials* **404**, 124057.

Liu, A., Liu, J., Han, J. & Zhang, W. 2017 Evolution of nanoscale zero-valent iron (nZVI) in water: Microscopic and spectroscopic evidence on the formation of nano- and micro-structured iron oxides. *Journal of Hazardous Materials* **322**, 129–135.

Liu, Y., Sheng, X., Zhou, Z., Wang, P., Lu, Z., Dong, J., Dong, J. & Lyu, S. 2021 Insight into naphthalene degradation by nano calcium peroxide in Fe(II)-citric acid catalytic environment. *Water, Air, & Soil Pollution* **232**, 503.

Mao, X., Jiang, R., Xiao, W. & Yu, J. 2015 Use of surfactants for the remediation of contaminated soils: A review. *Journal of Hazardous Materials* **285**, 419–435.

Mojiri, A., Zhou, J. L., Ohashi, A., Ozaki, N. & Kindaichi, T. 2019 Comprehensive review of polycyclic aromatic hydrocarbons in water sources, their effects and treatments. *Science of the Total Environment* **696**, 133971.

Ogbuagu, D. H., Okoli, C. G., Gilbert, C. L. & Madu, S. 2011 Determination of the contamination of groundwater sources in Okrika Mainland with polynuclear aromatic hydrocarbons (PAHs). *British Journal of Environment and Climate Change* **1** (3), 90–102.

Samrendra, S., Azhar, R., Kiran, S., Siddhartha, S., Anisa, R., Ajar, N., Subodh, K. & Shweta, Y. 2023 Polycyclic aromatic hydrocarbon (PAH)-contaminated soil decontamination through vermiremediation. *Water, Air, & Soil Pollution* **234**, 247.

Sheng, X. & Lyu, S. 2023 Insights into enhanced removal of fluoranthene by sulfidated nanoscale zero-valent iron: In aqueous solution and soil slurry. *Chemosphere* **312**, 137172.

Song, Y., Fang, G., Zhu, C., Zhu, F., Wu, S., Chen, N., Wu, T., Wang, Y., Gao, J. & Zhou, D. 2019 Zero-valent iron activated persulfate remediation of polycyclic aromatic hydrocarbon-contaminated soils: An in situ pilot-scale study. *Chemical Engineering Journal* **355**, 65–75.

Sun, Y., Li, M., Gu, X., Danish, M., Shan, A., Ali, M., Qiu, Z., Sui, Q. & Lyu, S. 2021 Mechanism of surfactant in trichloroethene degradation in aqueous solution by sodium persulfate activated with chelated-Fe(II). *Journal of Hazardous Materials* **407**, 124814.

Wang, J. & Wang, S. 2020 Reactive species in advanced oxidation processes: Formation, identification and reaction mechanism. *Chemical Engineering Journal* **401**, 126158.

Wang, F., Wu, Y., Gao, Y., Li, H. & Chen, Z. 2016 Effect of humic acid, oxalate and phosphate on Fenton-like oxidation of microcystin-LR by nanoscale zero-valent iron. *Separation and Purification Technology* **170**, 337–343.

Wang, L., Peng, L., Xie, L., Deng, P. & Deng, D. 2017 Compatibility of surfactants and thermally activated persulfate for enhanced subsurface remediation. *Environmental Science & Technology* **51** (12), 7055–7064.

Wu, C. & Linden, K. G. 2010 Phototransformation of selected organophosphorus pesticides: Roles of hydroxyl and carbonate radicals. *Water Research* **44** (12), 3585–3594.

Wu, W., Duan, H., Chen, J., Xu, J., Xu, F., Huang, T. & Xu, X. 2022 Catalytic effect of cyclohexanone combined with chloride ion activation of peroxomonosulfate to degrade acid orange 7. *Water, Air, & Soil Pollution* **233**, 381.

Xu, H., Gao, M., Hu, X., Chen, Y., Li, Y., Xu, X., Zhang, R., Yang, X., Tang, C. & Hu, X. 2021a A novel preparation of S-nZVI and its high efficient removal of Cr(VI) in aqueous solution. *Journal of Hazardous Materials* **416**, 125924.

Xu, Z., Huang, J., Fu, R., Zhou, Z., Ali, M., Shan, A., Yang, R., Zeng, G., Zhou, Z., Idrees, A. & Lyu, S. 2021b Enhanced trichloroethylene degradation in the presence of surfactant: Pivotal role of Fe (II)/nZVI catalytic synergy in persulfate system. *Separation and Purification Technology* **272**, 118885.

Yang, R., Zeng, G., Xu, Z., Zhou, Z., Huang, J., Fu, R. & Lyu, S. 2021 Comparison of naphthalene removal performance using H_2O_2, sodium percarbonate and calcium peroxide oxidants activated by ferrous ions and degradation mechanism. *Chemosphere* **283**, 131209.

Yu, S., Gu, X., Lu, S., Xue, Y., Zhang, X., Xu, M., Qiu, Z. & Sui, Q. 2018 Degradation of phenanthrene in aqueous solution by a persulfate/percarbonate system activated with CA chelated-Fe (II). *Chemical Engineering Journal* **333**, 122–131.

Zeng, G., Yang, R., Zhou, Z., Huang, J., Danish, M. & Lyu, S. 2022 Insights into naphthalene degradation in aqueous solution and soil slurry medium: Performance and mechanisms. *Chemosphere* **291**, 132761.

Zhou, Z., Huang, J., Xu, Z., Ali, M., Shan, A., Fu, R. & Lyu, S. 2021 Mechanism of contaminants degradation in aqueous solution by persulfate in different Fe(II)-based synergistic activation environments: Taking chlorinated organic compounds and benzene series as the targets. *Separation and Purification Technology* **273**, 118990.

First received 20 June 2023; accepted in revised form 1 January 2024. Available online 12 January 2024